Detection of Weak Microwave Fields with an Underdamped Josephson Junction

G. Oelsner,[1,*] C. K. Andersen,[2] M. Rehák,[3] M. Schmelz,[1] S. Anders,[1] M. Grajcar,[3] U. Hübner,[1] K. Mølmer,[2] and E. Il'ichev[1,4]

[1]*Leibniz Institute of Photonic Technology, P.O. Box 100239, D-07702 Jena, Germany*
[2]*Department of Physics and Astronomy, Aarhus University, DK-8000 Aarhus, Denmark*
[3]*Department of Experimental Physics, Comenius University, SK-84248 Bratislava, Slovakia*
[4]*Novosibirsk State Technical University, 20 Karl Marx Avenue, 630092 Novosibirsk, Russia*

(Received 23 May 2016; revised manuscript received 22 September 2016; published 19 January 2017)

We construct a microwave detector based on the voltage switching of an underdamped Josephson junction that is positioned at a current antinode of a $\lambda/4$ coplanar waveguide resonator. By measuring the switching current and the transmission through a waveguide capacitively coupled to the resonator at different drive frequencies and temperatures, we are able to fully characterize the system and assess its detection efficiency and sensitivity. Testing the detector by applying a classical microwave field with the strength of a single photon yields a sensitivity parameter of 0.5, in qualitative agreement with theoretical calculations.

DOI: 10.1103/PhysRevApplied.7.014012

I. INTRODUCTION

The light emission by single microscopic quantum systems displays a number of nonclassical features which have been exploited in fundamental investigations in quantum physics and which may result in applications in metrology, quantum communication, and computing. Potential applications, however, would suffer from the rather weak coupling between atoms and single optical photons. This consequence has stimulated efforts to study the same features with macroscopic artificial atoms. A particularly successful system relies on solid-state superconducting circuits. Because of the Josephson nonlinearity, such circuits have an anharmonic excitation spectrum and may be restricted to an effective two-level system which can interact resonantly with microwave fields. Besides the stronger coupling of superconducting circuits, an additional advantage is that they can be designed and fabricated on chip scale, thereby allowing the integration in and scaling to larger systems with multiple components.

Essential quantum-optical effects with superconducting qubits, such as vacuum Rabi splitting [1], resonance fluorescence of a single artificial atom [2], and single-atom lasing [3] have already been observed. Microwave fields can be amplified, detected, and fully characterized in homodyne setups [4]. The effective coupling to transmission waveguides has made it possible to efficiently monitor the emitted radiation and verify the validity of the quantum trajectories of qubits conditioned on the detection record [5,6], as well as to apply feedback and stabilize coherent superposition states of the qubit [7].

Quantum optics benefits from high-efficiency single-photon detectors. It relies on the energy of the individual photons being sufficient to exploit the photoelectric effect and liberate an electron which can be amplified and detected [8]. Transition-edge sensors [9] and superconducting nanowire single-photon detectors [10,11] also require a sufficiently large energy of the incident photon to heat and thus modify the current through the detector. For the detection of weak incident microwave fields, promising results have been obtained recently by the use of thermometry at superconductor–normal-metal–superconductor [12] and normal-metal–insulator–superconductor [13] junctions.

Still, with present technology, a general-purpose detector for single microwave photons is not possible due to the low energy associated with photons in the microwave regime. However, a few ideas for work-arounds exist. For the creation and detection, a qubit is a natural component to consider when interested in single-photon dynamics, as qubits inherently work in the single-excitation regime. Indeed, the creation of single photons has been demonstrated by transferring the excitation from an excited qubit to a cavity [14,15] and to an emission line [16]. A possible photon detector could work by the absorbtion of a photon by a qubit and then reading out the qubit state [17,18]. The phase qubit is therefore of particular interest as the qubit supports a built-in readout process [19,20]. The phase qubit is a current-biased Josephson junction (CBJJ) [21–23] operated in a regime of only two bound states. Recent works using a CBJJ have made progress towards a single microwave-photon detector [22,24–26]. This work expands on this progress.

A CBJJ is a device of particular interest since the phase variable associated with the junction acts as a particle

*gregor.oelsner@leibniz-ipht.de

trapped in a washboard potential. The properties of the CBJJ are, however, modified by even a weak probe field and may therefore directly measure an incident microwave field. The experiment presented here uses the tunneling events in a CBJJ as a photon detector in the few-photon regime by coupling the CBJJ to a $\lambda/4$ resonator. The general idea is to use the device both as a collector of photons and as a detector, sensitive to a single or a few quanta in the resonator through a classical measurable response in the form of a voltage switch over the Josephson junction. The major difference between the approach discussed in this work and that addressed in Refs. [22,26] is that the detection here is not due to the resonant interaction between a single CBJJ (operated as a phase qubit) and a photon, which produces a signal governed by the photon number. In contrast, the tunneling properties of the CBJJ are directly affected by the strong coupling to the current amplitude of the resonator and depend on the microwave-photon number only via its relation to the field amplitude. This difference makes the appropriate theoretical treatment much different. A phase qubit requires only two states to be properly described, but, for a CBJJ coupled (possibly off resonantly) to the field of a resonator, many levels may be relevant. Furthermore, the switching dynamics can no longer be described as a simple incoherent decay from the two qubit levels, but it must be described as a resonator field-dependent process. Furthermore, the current device may result in several operational advantages. (i) With the detector operating as a qubit, it can inherently only measure one photon, but, using the current setup, a threshold for any number of photons in the field can be set, allowing for a wider spectrum of applications. (ii) The bandwidth of the detector is more directly controlled since engineering a capacitive coupling to a resonator is straightforward. (iii) For the CBJJ to work well as a qubit, the bias current must be tuned to a specific value. For our setup, the resonator frequency depends only weakly on the bias current. (iv) A phase qubit is often dominated by a very large decoherence rate, which limits its detector efficiency. (v) A resonator is more convenient to incorporate in a modular fashion in larger circuits. For instance, one can imagine an additional qubit being dispersively coupled to the resonator such that this device now also works as a qubit readout device.

II. SAMPLE AND EXPERIMENTAL SETUP

In Ref. [27], we used a quantum trajectory treatment to analyze the performance of such a system comprised of a $\lambda/4$ coplanar waveguide resonator shunted to ground via a Josephson junction, and here we demonstrate a prototype of such a device and report on its performance. We design and fabricate a superconducting circuit that consists of two $\lambda/4$ waveguides, both shunted to ground via a Josephson junction. The chip layout, together with light-microscope

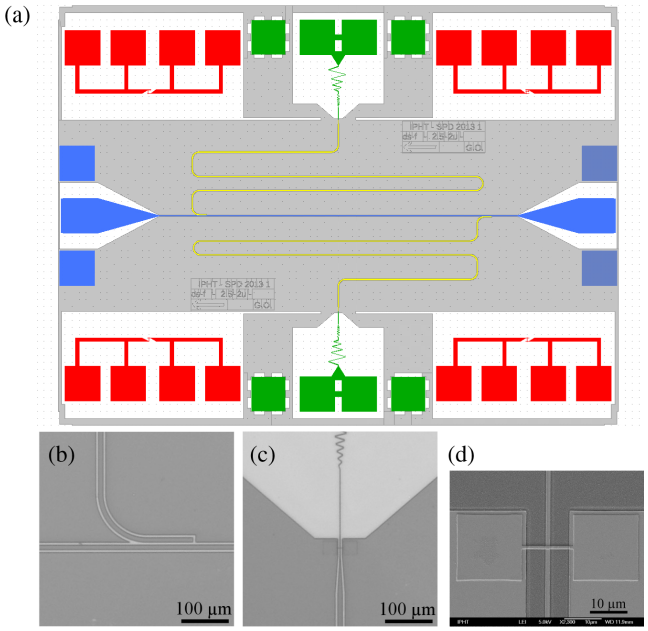

FIG. 1. (a) An (8×6)-cm sample is displayed as a colored design picture consisting of a central conduction line (blue), two coupled $\lambda/4$ resonators (yellow), dc connections to the Josephson junctions (green), and test junction circuits in the corners of the chip (red). (b) A LM micrograph of the coupling capacitance of the upper resonator. The central conductor and the resonators are formed by coplanar lines. (c) LM micrograph of the junction's position in the resonator current antinode. From the top-central point, the dc-bias line is visible. Beyond the junction, it continues as a central resonator line with a ground plane on each side. (d) SEM image of the Josephson junction shunting the resonator in its current antinode. The barbell-like structure is a layer of Nb deposited on top of the structured trilayer that forms the rest of the circuit, and the Josephson junctions are found in the overlap.

(LM) micrographs of selected parts and a SEM image of one of the Josephson junctions is shown in Fig. 1. For the application of microwave signals and for the characterization of the system, a transmission line is capacitively coupled to the resonators. The coupling capacitance is estimated to be $C_c = 10$ fF from a full electromagnetic finite-element simulation. The length of the resonators is chosen for a center frequency of the fundamental resonance of about 2.5 GHz. A slight length difference is introduced to detune their resonant frequencies by about 60 MHz to allow the individual characterization of each device [28]. The sample is fabricated on a silicon substrate using the cross-type $Nb/AlO_x/Nb$ fabrication process [29] with a target critical current density of 200 A/cm^2. The output (gap) voltage of the Josephson junctions takes a value of 2.8 mV, and no additional amplifiers are necessary for detection. The sample is placed in a dilution refrigerator with a base temperature of about 15 mK. The external noise is reduced by magnetic and superconducting shielding, together with heavy filtering of the input and output signal lines. To estimate the influence of the external dc lines on

the microwave properties of the oscillators, we bond only one junction to the external lines.

III. EXPERIMENTAL CHARACTERIZATION

With a first set of experiments, we determine the parameters of the subsystems. First, we measure the transmission of the central transmission line at different frequencies, and we find two resonances, at $\omega_1/2\pi = 2.506$ GHz and $\omega_2/2\pi = 2.44$ GHz, with similar quality factors Q of about 1000. Thus, we conclude that no significant additional losses are introduced by connection of the resonator and the junction to the dc circuitry. By applying a dc-bias current to the connected Josephson junction, we are able to measure its resonance frequency ω_1 shift to lower values; see the lower panel in Fig. 2.

The Josephson inductance is a function of the bias current, $L_J = \Phi_0/(2\pi\sqrt{I_c^2 - I^2})$, where Φ_0 is the magnetic flux quantum. Therefore, the total resonator inductance $L_t = L_E + L_J$ also depends on I. By making use of the lumped element representation of the oscillator, we obtain an equation for its resonance frequency,

$$\omega_1 = \frac{1}{\sqrt{C_E(L_E + L_J)}}. \quad (1)$$

By fitting this expression to the data, we are able to extract the effective resonator capacitance $C_E = 1.6 \pm 0.05$ pF, its inductance $L_E = 2.49 \pm 0.07$ nH, and the critical current, $I_c = 13.8 \pm 0.08$ μA. The error bars represent the 95% confidence bounds of the fitted values. Knowing these parameters, we can estimate the mean amplitude of the current $I_{\rm ph} \approx \sqrt{\hbar\omega_1/L_E} = 25$ nA produced by a single photon in the resonator. Note that vacuum fluctuations are of the same

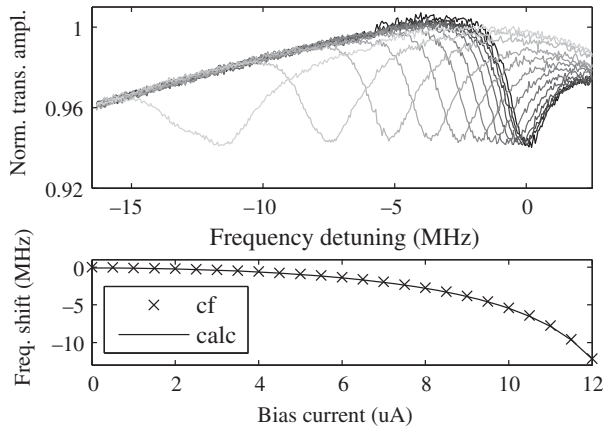

FIG. 2. (Upper panel) The normalized transmission amplitude as a function of the probing frequency. From dark to light curves, the dc-bias current at the junction is increased in steps of 1 μA. The crosses in the lower panel show the center frequency (cf) shifts as a function of the bias current. They are found by fitting the transmission dips in the upper panel to Lorentzian line shapes. The measured frequency shifts are in excellent agreement with the analytical fit in Eq. (1) (the solid line).

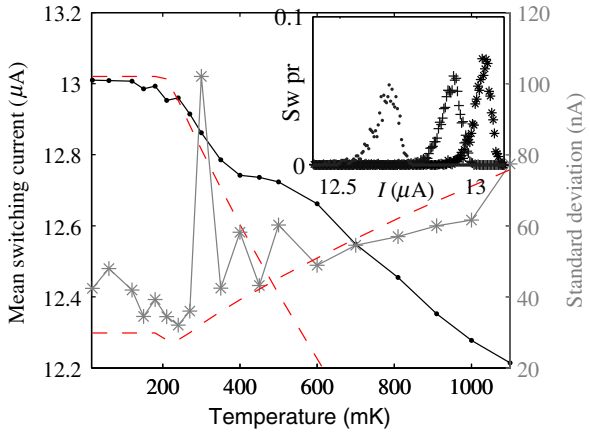

FIG. 3. Mean switching current (the black curve) and standard deviation (the gray curve) of the switching-current histograms at different temperatures. The dashed red curves correspond to theoretical curves calculated as in Ref. [30]. While the temperature dependence of the standard deviation is reproduced quite well, the mean switching currents are underestimated by theory. The large variation around 300–500 mK is most probably due to additional noise present during the measurement time. (Inset) Examples of the histograms [the switching probability (sw pr) over the bias current] at temperatures of 600, 300, and 14 mK, marked by points, crosses, and stars, respectively.

order of magnitude, and therefore it is important that we characterize the actual difference of the response of the device for the vacuum and weak microwave fields [27].

In the next series of experiments, we determine the switching current distributions under different experimental conditions by ramping up the current with a rate of 0.5 μA/s and recording the values at which the junction switches to the finite-voltage state. The extracted values for the mean switching current and their standard deviations σ are plotted in Fig. 3 for different temperatures of the chip. At the lowest temperatures, we find the largest values of the switching current I_m of about 13 μA, with a standard deviation σ of 40 nA. The measured switching currents are in qualitative agreement with the expected temperature dependence [30], although the steepness of the expected mean value is overestimated (possibly because of the resonator coupling). Specifically, we observe a crossover from a quantum to a thermally activated tunneling regime at around 200 mK, which is consistent with a normal resistance of $R_J = 140\,\Omega$ and a capacitance of $C_J = 400$ fF [29], estimated from the junction size and geometry.

IV. SENSITIVITY

These experiments all serve as characterization of the system parameters. Now we use the device to sense a weak microwave field. The application of a driving signal $V_{\rm in}\sin\omega_p t$ yields a resonator driving amplitude of $\Omega_d = C_c V_{\rm in} V_0/2\hbar$. Here, $V_{\rm in}$ is the input voltage amplitude at the coupling capacitance and $V_0 = \sqrt{\hbar\omega_1/C_E}$ the

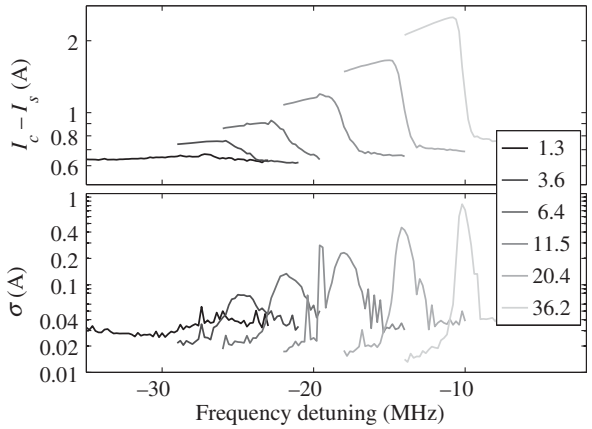

FIG. 4. Influence of microwave signals on the switching-current histograms. The difference between the mean switching and critical currents $I_c - I_s$ in the upper as well as the standard deviation σ of the switching current in the lower picture is measured for different driving frequencies. From light to dark, the driving amplitude is decreased according to the legend in megahertz.

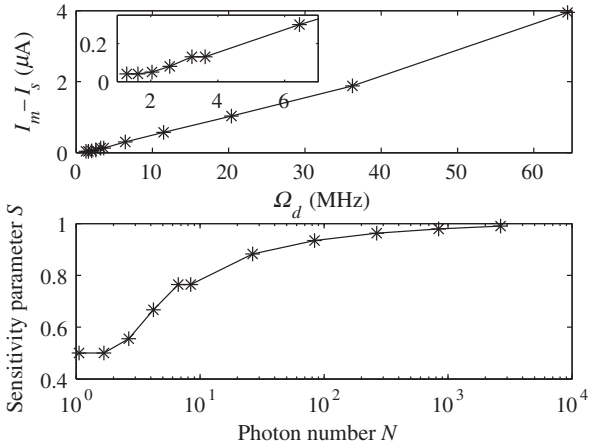

FIG. 5. (Upper plot) Maximal shift of the mean switching current at different driving amplitudes Ω_d. (Inset) Enlargement of the region close to zero driving. (Lower plot) Reconstructed sensitivity of our detector as the extracted maximal shift of the histograms divided by the shift plus the standard deviation of the switching current of the undisturbed junction. The mean photon number in the resonator N on the x axis follows from the driving amplitudes Ω_d.

zero-point voltage of the resonator. In the experiments, carried out at 15 mK, we ramp the bias current, observe the switching behavior, and record the switching-current distributions as functions of the applied microwave frequency and amplitude.

In Fig. 4, the different curves display the frequency dependence of the mean switching current (upper panel) and its standard deviation (lower panel) for different values of the applied amplitude. The curves appear from left to right according to the increasing values of the amplitude indicated. The curves for different amplitudes all show a similar dependence on the frequency detuning.

The overall frequency dependence can be explained by the shift of the resonance curve with increasing bias current (see Fig. 2). To detect a given amplitude of the rf signal, the bias current must attain a specific value such that the additional rf current suffices to switch the junction to the finite-voltage state. Because of the nonlinear Josephson inductance, this bias current shifts the resonator frequency, and hence the optimal input coupling is achieved at the shifted resonance condition of the resonator. When decreasing the frequency for large amplitude driving, we obtain a standard deviation with a minimum that lies below the one for the undisturbed junction. We obtain this result because the strong driving allows excitation directly into the continuum that is represented by the voltage state, in addition to the switching by tunneling [23].

Finally, from the same experimental data, we extract the dependence of the maximal shifts of the mean switching currents as a function of the driving amplitude and the corresponding photon number in the resonator (see Fig. 5). For the device to work as a detector of single photons, the design needs to be tailored such that the sensitivity is maximal at the frequency of the photons. The bandwidth of the detector is then set by the linewidth appearing in Fig. 4.

The upper panel of Fig. 5 displays a linear dependence of the maximal shift of the mean switching currents on the driving amplitude. This linearity indicates that the switching to the voltage state that leads to the detection is, indeed, caused by the modulation of the junction potential by the rf current in the coupled resonator and junction system [27], and not just by resonance between the applied microwave and the qubit.

In the upper plot of Fig. 6, we show the switching-current distributions for the undisturbed and the weakly

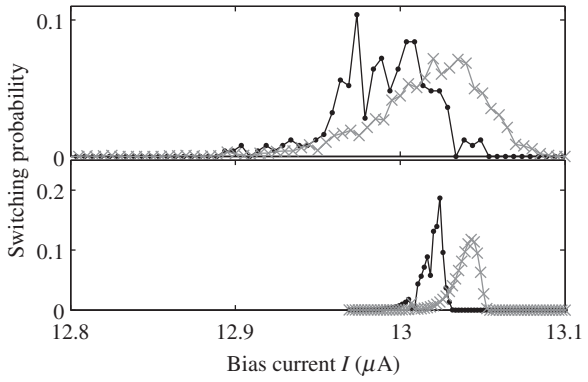

FIG. 6. (Upper panel) The measured undisturbed histogram (the gray crosses) compared to the maximally shifted histograms for the lowest applied driving power (the black dots). They have a Hellinger distance [31] of 0.51. For comparison, the theoretical predictions are shown in the lower panel for the same parameters. The histograms shifted by the microwave signal in both cases show a characteristic peak structure.

driven junction. To estimate whether the detector is illuminated with a given field strength or not by a single measurement of the switching current, one merely identifies which of the two candidate switching-current probability distributions is larger at the value measured. The accomplishment of that procedure, averaged over the possible outcomes, is quantified statistically, e.g., by the Hellinger distance [31] between the distributions. For Gaussian distributions, this distance is given analytically by their widths and separation and, for simplicity, we shall characterize our (non-Gaussian) distributions by a width σ and by their mean values I_m and I_s. Because the width of the histograms prevents a precise identification of the switching current I_s, the amplitude signal-to-noise ratio can then be defined as $\mathrm{SNR} = (I_m - I_s)/\sigma$. This definition motivates the assignment of the sensitivity parameter, $S = \mathrm{SNR}/(\mathrm{SNR} + 1)$, denoting how well we can distinguish whether a drive is applied. With the loss rate $\kappa = \omega_1/Q$, the mean number of photons $N = 4\Omega_d^2/\kappa^2$ inside the resonator can be assigned to a driving amplitude Ω_d [32]. By plotting S as a function of the photon number in the lower panel of Fig. 5, we find a SNR of 1 and a value of $S = 0.5$ for a drive strength corresponding to a single microwave photon in the resonator.

V. COMPARISON TO THEORY

We use the theory developed in Refs. [23,27] to calculate the effective potential from which we directly found a switching rate [33], both when applying a weak field and without any drive. Using these rates, we calculate the results shown in the corresponding lower panel of Fig. 6, which are equivalent to the measured results in the upper plot. While the theory produces a narrower distribution ($\sigma = 10$ nA), it qualitatively reproduces the experimental data and we calculate a sensitivity of 0.65 in the single-photon regime. The broader distribution of the experiment is most likely due to the multimode structure of the resonator. In Ref. [27], we explicitly neglected higher modes, as both the resonator and the CBJJ were far detuned from these modes. However, in the experiment, the CBJJ is also far detuned from the probed mode, and thus we expect the CBJJ to interact equivalently with several modes. This additional interaction effectively introduces another decay channel of the resonator that is not taken into account in the theory and leads to a broader switching distribution. Notably, we find that the theory directly reproduces a spiked structure of the switching-current distribution for the driven detector also seen in the measured results, which confirms that this structure indeed is related to the coupling between the resonator and the current-biased Josephson junction. The theory also predicts that we may achieve a higher sensitivity for a device with a smaller critical current. The detection also works nicely for strong microwave signals and, after calibration at a fixed frequency detuning in Fig. 4, we can conclude that the device can be used to infer the intensity of the drive signal.

VI. DISCUSSION

The current device does has a few drawbacks compared to an all-purpose single-photon detector in the microwave regime. As identified by employing the theory in Ref. [27], the resonator's lifetime must be larger than the tunneling time of the CBJJ, set by the effective coupling of the resonator to the CBJJ. This qualification requires a Q factor of around 1000, and thus the device will measure microwave fields within a frequency bandwidth of only a few megahertz. This value, however, is not so different from the bandwidth of linear quantum-limited amplifiers [34–37]. A more detrimental drawback is the initialization time and the related dead time of the detector. The detector works by having the bias current slowly ramped up from 0. This ramping takes seconds in order to avoid nonadiabatic excitations in the CBJJ. Similarly, once the detector switches, it must be reset by setting the current back to 0 and waiting approximately milliseconds for the quasiparticles to leave the CBJJ. This requirement implies a very low repetition rate for experiments using this detector.

While the current experimental device is far from a perfect photon detector, we may consider setups where the present detector may be preferable to the homodyne or heterodyne detection schemes commonly used in circuit QED. Such an experiment could be a microwave analogy of a Hanbury Brown and Twiss (HBT) experiment [38]. In a HBT experiment, a source of light is split on a beam splitter and correlations between measurements of the two output fields reveal photon statistics of the input field. With photon detectors at the outputs, the two-time correlation function between the two signals is denoted $G^2(\tau) = \langle \mathcal{I}_1(t)\mathcal{I}_2(t-\tau)\rangle$, with $\mathcal{I}_i(t)$ being the intensity at detector i. Now, if the input field is a single-photon field (as opposed to a coherent field), the correlation function vanishes for simultaneous detection, i.e., $G^2(0) = 0$, which would not be true for a coherent field. This effect for single photons is known as antibunching. A microwave analogy of such an experiment was performed in Ref. [39] by using linear amplifiers and heterodyne detection. The linear signal does, obviously, contain signatures of antibunching, but only by recording many (in the order of 10^5) time trajectories does the statistics of the classical signals reveal the G^2 function of the single photons [4]. A similar experiment can be performed with two of our detectors. Here, the bias currents of both detectors are slowly ramped up as in the current experiments, and the joint switching-current distributions $P_Q(I_{b1}, I_{b2})$ and $P_C(I_{b1}, I_{b2})$ can be recorded for a single-photon source or a coherent drive with a single photon, on average, respectively. Similarly, we have a joint distribution

function $P_0(I_{b1}, I_{b2})$ measured with no input signal. Then we find the relation $G^2(0) \propto \langle (P_Q - P_0)/(P_C - P_0) \rangle_{I_{b1}=I_{b2}}$ and thus we can directly observe the antibunching of microwave photons, an effect that was previously only inferred indirectly [39]. However, because of the long initialization and dead times of the detector, the measurement time to obtain sufficient data for calculating the G^2 function would still be comparable to the total time using quantum-limited linear detectors in the setup used in Ref. [39].

VII. CONCLUSION

In this work, we develop the prototype of a device that may be used for the determination of classical field amplitudes in the microwave domain. Our device achieves a sensitivity parameter of 0.5 in the low photon limit. This value is in agreement with the expected signal level of single photons, and it may be improved by altering the design. For example, the width of the switching-current distributions may be decreased and, for the values achieved in Ref. [30], a sensitivity parameter of the order of unity can be expected at the single-photon level. Furthermore, the input coupling of the cavity may be optimized and the resonator can be matched to fit the impedance of standard transmission lines and thus can avoid reflections. Based on the work presented here, such optimized devices are currently under development in our laboratory and will be made the subject of future investigations.

ACKNOWLEDGMENTS

The research leading to these results has received funding from the European Community Seventh Framework Programme (FP7/2007-2013) under Grant No. 270843 (iQIT). C. K. A. and K. M. acknowledge the financial support from the Villum Foundation. M. G. and M. R. acknowledge partial support from the Slovak Research and Development Agency under Contracts No. APVV-0808-12 and No. APVV-0088-12. E. I. acknowledges partial support from the Russian Ministry of Education and Science, within the framework of State Assignment No. 8.337.2014/K.

[1] A. Wallraff, D. I. Schuster, A. Blais, L. Frunzio, R.-S. Huang, J. Majer, S. Kumar, S. M. Girvin, and R. J. Schoelkopf, Strong coupling of a single photon to a superconducting qubit using circuit quantum electrodynamics, Nature (London) **431**, 162 (2004).

[2] O. Astafiev, A. M. Zagoskin, A. A. Abdumalikov, Jr., Yu. A. Pashkin, T. Yamamoto, K. Inomata, Y. Nakamura, and J. S. Tsai, Resonance fluorescence of a single artificial atom, Science **327**, 840 (2010).

[3] O. Astafiev, K. Inomata, A. O. Niskanen, Yu. A. Pashkin, T. Yamamoto, K. Inomata, Y. Nakamura, and J. S. Tsai, Single artificial-atom lasing, Nature (London) **449**, 588 (2007).

[4] M. P. da Silva, D. Bozyigit, A. Wallraff, and A. Blais, Schemes for the observation of photon correlation functions in circuit QED with linear detectors, Phys. Rev. A **82**, 043804 (2010).

[5] K. W. Murch, S. J. Weber, C. Macklin, and I. Siddiqi, Observing single quantum trajectories of a superconducting quantum bit, Nature (London) **502**, 211 (2013).

[6] P. Campagne-Ibarcq, P. Six, L. Bretheau, A. Sarlette, M. Mirrahimi, P. Rouchon, and B. Huard, Observing Quantum State Diffusion by Heterodyne Detection of Fluorescence, Phys. Rev. X **6**, 011002 (2016).

[7] R. Vijay, C. Macklin, D. H. Slichter, S. J. Weber, K. W. Murch, R. Naik, A. N. Korotkov, and I. Siddiqi, Stabilizing Rabi oscillations in a superconducting qubit using quantum feedback, Nature (London) **490**, 77 (2012).

[8] R. H. Hadfield, Single-photon detectors for optical quantum information applications, Nat. Photonics **3**, 696 (2009).

[9] M. Förtsch, T. Gerrits, M. J. Stevens, D. Strekalov, G. Schunk, J. U. Fürst, U. Vogl, F. Sedlmeir, H. G. L. Schwefel, G. Leuchs, S. W. Nam, and C. Marquardt, Near-infrared single-photon spectroscopy of a whispering gallery mode resonator using energy-resolving transition edge sensors, J. Opt. **17**, 065501 (2015).

[10] C. M. Natarajan, M. G. Tanner, and R. H. Hadfield, Superconducting nanowire single-photon detectors: Physics and applications, Supercond. Sci. Technol. **25**, 063001 (2012).

[11] O. Kahl, S. Ferrari, V. Kovalyuk, G. N. Goltsman, A. Korneev, and W. H. Pernice, Waveguide integrated superconducting single-photon detectors with high internal quantum efficiency at telecom wavelengths, Sci. Rep. **5**, 10941 (2015).

[12] J. Govenius, R. E. Lake, K. Y. Tan, V. Pietilä, J. K. Julin, I. J. Maasilta, P. Virtanen, and M. Möttönen, Microwave nanobolometer based on proximity Josephson junctions, Phys. Rev. B **90**, 064505 (2014).

[13] S. Gasparinetti, K. L. Viisanen, O.-P. Saira, T. Faivre, M. Arzeo, M. Meschke, and J. P. Pekola, Fast Electron Thermometry for Ultrasensitive Calorimetric Detection, Phys. Rev. Applied **3**, 014007 (2015).

[14] A. A. Houck, D. I. Schuster, J. M. Gambetta, J. A. Schreier, B. R. Johnson, J. M. Chow, L. Frunzio, J. Majer, M. H. Devoret, S. M. Girvin, and R. J. Schoelkopf, Generating single microwave photons in a circuit, Nature (London) **449**, 328 (2007).

[15] M. Pechal, L. Huthmacher, C. Eichler, S. Zeytinoğlu, A. A. Abdumalikov, Jr., S. Berger, A. Wallraff, and S. Filipp, Microwave-Controlled Generation of Shaped Single Photons in Circuit Quantum Electrodynamics, Phys. Rev. X **4**, 041010 (2014).

[16] Z. H. Peng, J. S. Tsai, and O. V. Astafiev, Tuneable on-demand single-photon source in the microwave range, Nat. Commun. **7**, 12588 (2016).

[17] K. Inomata, Z. Lin, K. Koshino, W. D. Oliver, J.-S. Tsai, T. Yamamoto, and Y. Nakamura, Single microwave-photon detector using an artificial Λ-type three-level system, Nat. Commun. **7**, 12303 (2016).

[18] A. Narla, S. Shankar, M. Hatridge, Z. Leghtas, K. M. Sliwa, E. Zalys-Geller, S. O. Mundhada, W. Pfaff, L. Frunzio,

R. J. Schoelkopf, and M. H. Devoret, Robust Concurrent Remote Entanglement between Two Superconducting Qubits, Phys. Rev. X **6**, 031036 (2016).

[19] John M. Martinis, S. Nam, J. Aumentado, and C. Urbina, Rabi Oscillations in a Large Josephson-Junction Qubit, Phys. Rev. Lett. **89**, 117901 (2002).

[20] A. J. Berkley, H. Xu, R. C. Ramos, M. A. Gubrud, F. W. Strauch, P. R. Johnson, J. R. Anderson, A. J. Dragt, C. J. Lobb, and F. C. Wellstood, Entangled macroscopic quantum states in two superconducting qubits, Science **300**, 1548 (2003).

[21] M. Weides, R. C. Bialczak, M. Lenander, E. Lucero, Matteo Mariantoni, M. Neeley, A. D. O'Connell, D. Sank, H. Wang, J. Wenner, T. Yamamoto, Y. Yin, A. N. Cleland, and J. Martinis, Phase qubits fabricated with trilayer junctions, Supercond. Sci. Technol. **24**, 055005 (2011).

[22] Y. F. Chen, D. Hover, S. Sendelbach, L. Maurer, S. T. Merkel, E. J. Pritchett, F. K. Wilhelm, and R. McDermott, Microwave Photon Counter Based on Josephson Junctions, Phys. Rev. Lett. **107**, 217401 (2011).

[23] C. K. Andersen and K. Mølmer, Effective description of tunneling in a time-dependent potential with applications to voltage switching in Josephson junctions, Phys. Rev. A **87**, 052119 (2013).

[24] G. Romero, J. J. Garcia-Ripoll, and E. Solano, Microwave Photon Detector in Circuit QED, Phys. Rev. Lett. **102**, 173602 (2009).

[25] B. Peropadre, G. Romero, G. Johansson, C. M. Wilson, E. Solano, and J. J. Garcia-Ripoll, Approaching perfect microwave photodetection in circuit QED, Phys. Rev. A **84**, 063834 (2011).

[26] A. Poudel, R. McDermott, and M. G. Vavilov, Quantum efficiency of a microwave photon detector based on a current-biased Josephson junction, Phys. Rev. B **86**, 174506P (2012).

[27] C. K. Andersen, G. Oelsner, E. Il'ichev, and K. Mølmer, Quantized resonator field coupled to a current-biased Josephson junction in circuit QED, Phys. Rev. A **89**, 033853 (2014).

[28] M. Jerger, S. Poletto, P. Macha, U. Hübner, A. Lukashenko, E. Il'ichev, and A. V. Ustinov, Readout of a qubit array via a single transmission line, Europhys. Lett. **96**, 40012 (2011).

[29] S. Anders, M. Schmelz, L. Fritzsch, R. Stolz, V. Zakosarenko, T. Schönau, and H.-G. Meyer, Sub-micrometer-sized, cross-type Nb-AlOx-Nb tunnel junctions with low parasitic capacitance, Supercond. Sci. Technol. **22**, 064012 (2009).

[30] G. Oelsner, L. S. Revin, E. Il'ichev, A. L. Pankratov, H. G. Meyer, L. Grönberg, J. Hassel, and L. S. Kuzmin, Underdamped Josephson junction as a switching current detector, Appl. Phys. Lett. **103**, 142605 (2013).

[31] D. Spehner, Quantum correlations and distinguishability of quantum states, J. Math. Phys. (N.Y.) **55**, 075211 (2014).

[32] S. N. Shevchenko, G. Oelsner, Ya. S. Greenberg, P. Macha, D. S. Karpov, M. Grajcar, U. Hübner, A. N. Omelyanchouk, and E. Il'ichev, Amplification and attenuation of a probe signal by doubly dressed states, Phys. Rev. B **89**, 184504 (2014).

[33] A. O. Caldeira and A. J. Leggett, Influence of Dissipation on Quantum Tunneling in Macroscopic Systems, Phys. Rev. Lett. **46**, 211 (1981).

[34] M. A. Castellanos-Beltran, K. D. Irwin, G. C. Hilton, L. R. Vale, and K. W. Lehnert, Amplification and squeezing of quantum noise with a tunable Josephson metamaterial, Nat. Phys. **4**, 929 (2008).

[35] C. Eichler and A. Wallraff, Controlling the dynamic range of a Josephson parametric amplifier, EPJ Quantum Technol. **1**, 1 (2014).

[36] M. Hatridge, R. Vijay, D. H. Slichter, John Clarke, and I. Siddiqi, Dispersive magnetometry with a quantum limited SQUID parametric amplifier, Phys. Rev. B **83**, 134501 (2011).

[37] N. Bergeal, F. Schackert, M. Metcalfe, R. Vijay, V. E. Manucharyan, L. Frunzio, D. E. Prober, R. J. Schoelkopf, S. M. Girvin, and M. H. Devoret, Phase-preserving amplification near the quantum limit with a Josephson ring modulator, Nature (London) **465**, 64 (2010).

[38] R. H. Brown and R. Q. Twiss, Correlation between photons in two coherent beams of light, Nature (London) **177**, 27 (1956).

[39] D. Bozyigit, C. Lang, L. Steffen, J. M. Fink, C. Eichler, M. Baur, R. Bianchetti, P. J. Leek, S. Filipp, M. P. da Silva, A. Blais, and A. Wallraff, Antibunching of microwave-frequency photons observed in correlation measurements using linear detectors, Nat. Phys. **7**, 154 (2011).